Hindawi Publishing Corporation
Journal of Nanomaterials
Volume 2014, Article ID 801562, 7 pages
http://dx.doi.org/10.1155/2014/801562

Research Article

High Cycling Performance Cathode Material: Interconnected $LiFePO_4$/Carbon Nanoparticles Fabricated by Sol-Gel Method

Zhigao Yang and Shengping Wang

Faculty of Material Science and Chemistry, China University of Geosciences, Wuhan 430074, China

Correspondence should be addressed to Shengping Wang; spwang@cug.edu.cn

Received 8 April 2014; Accepted 22 May 2014; Published 12 June 2014

Academic Editor: Hongmei Luo

Interconnected $LiFePO_4$/carbon nanoparticles for Li-ion battery cathode have been fabricated by sol-gel method followed by a carbon coating process involving redox reactions. The carbon layers coated on the $LiFePO_4$ nanoparticles not only served as a protection layer but also supplied fast electrons by building a 3D conductive network. As a cooperation, $LiFePO_4$ nanoparticles encapsulated in interconnected conductive carbon layers provided the electrode reactions with fast lithium ions by offering the lithium ions shortening and unobstructed pathways. Field emission scanning electron microscopy (FESEM) and X-ray diffraction (XRD) tests showed optimized morphology. Electrochemical characterizations including galvanostatic charge/discharge, cyclic voltammetry (CV), and electrochemical impedance spectroscopy (EIS) tests, together with impedance parameters calculated, all indicated better electrochemical performance and excellent cycling performance at high rate (with less than 9.5% discharge capacity loss over 2000 cycles, the coulombic efficiency maintained about 100%).

1. Introduction

Reported by Goodenough and coworkers for the first time in 1997, the phosphate polyanionic compound of $LiFePO_4$ shows superior performance including a high theoretical capacity (170 mAh g^{-1}) and an acceptable operating voltage (3.45 V versus Li^+/Li) [1, 2]. However, the slow diffusivity of Li^+ in $LiFePO_4$ (ca. 10^{-14} cm^2 s^{-1}) and the low electronic conductivity (ca. 10^{-9} S cm^{-1}) [3] restrict the high rate performance of $LiFePO_4$. Generally, carbon coating, nanocrystallization, and doping are main techniques to modify $LiFePO_4$. Although doping improved the performance of $LiFePO_4$ in some researches, the mechanism had not been clearly explained yet. Furthermore, there are some problems about the balance of charge and energy raising after doping to be taken into further consideration [4, 5]. Carbon coating can significantly improve the electrical conductivity [6–8] and reduce particle size as well as avoiding particle aggregation [9], nanocrystallization shortening the pathway of Li^+ [10], and mitigating the problem of slow Li^+ transport in the solid state. Thus, aiming at improving the low conductivity and slow diffusivity of Li^+ at the same time, many modification researches are conducted based on the combination of carbon coating (or carbon-decorating) and nanocrystallization [6, 11, 12]. However, the high surface energy of nanosized materials causes the problem of agglomeration, making the efforts of fabricating nanomaterials in vain [13]. This warns us that the carbon coating process should better take place accompanying the formation of nanoparticles or their precursors. Heterogeneous distribution of carbon and $LiFePO_4$ results in limited utilization of the $LiFePO_4$ active material [14], which emphasizes the importance of the quality of carbon layer (including the integrity, uniformity, and thickness). In order to make full use of the synergistic effect of carbon coating and nanocrystallization, structure of complete and uniform carbon layer coated on every single $LiFePO_4$ nanoparticle is highly desirable [15, 16]. For us, that means only a carbon coating process which happens during the formation of $LiFePO_4$ (or $LiFePO_4$ precursor) nanoparticles and resulting uniform, compact, and intact carbon layers can notably enhance the electrochemical performance of $LiFePO_4$ nanoparticles (especially the cycling and rate performances).

The interconnected $LiFePO_4$/carbon nanoparticles reported here possess the target structure (structure of complete and uniform carbon layer coated on every single

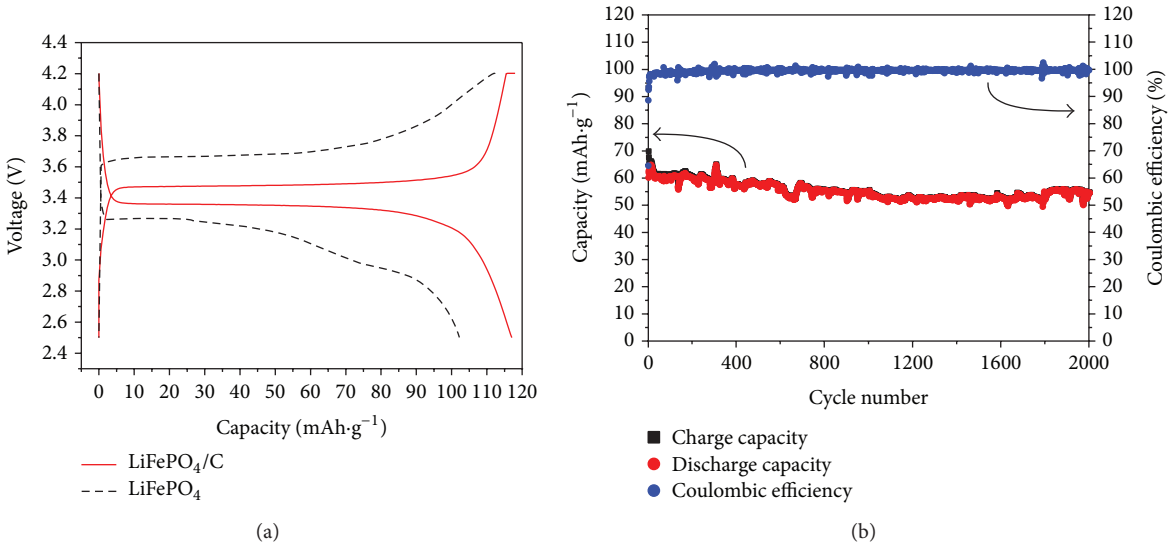

FIGURE 1: (a) Discharge/charge voltage profiles cycled at the 2nd cycle of $LiFePO_4$ and $LiFePO_4$/C at a current density of 34 mA g^{-1} (0.2 C). (b) Cycling performance of interconnected $LiFePO_4$/C nanoparticles at a current density of 850 mA g^{-1} (5 C).

$LiFePO_4$ nanoparticle) and exhibit commendable cycling performance at high rate.

2. Experimental

2.1. Fabrication of Bare $LiFePO_4$. The raw materials (all the chemical reagents used were obtained from Sinopharm Chemical Reagent Co., Ltd, China) for synthesizing the $LiFePO_4$ are P_2O_5, LiCl, and $FeSO_4{\cdot}7H_2O$. With continuous stirring, 7.0970 g (0.05 mol) of P_2O_5 was dissolved into 50 mL absolute ethyl alcohol to form solution A, and 4.4621 g (0.1 mol) of LiCl was dissolved into 100 mL absolute ethyl alcohol to form solution B. After 27.8020 g (0.1 mol) of $FeSO_4{\cdot}7H_2O$ was added into 100 mL absolute ethyl alcohol, solution A and solution B were added into it with the volume ratio of 1 : 2 while stirring. Then the solution was covered with plastic film and stirred for 3 hours to form a uniform sol. After stirring in the 65°C water bath without plastic film for several hours, the gel was formed. Finally, sucrose (A reducing atmosphere was created by thermal decomposition of the sucrose at the upstream) and as-prepared gel were put in a magnetic boat with the mass ratio of 1 : 10 to undergo the calcining process at 700°C in argon atmosphere for 8 hours. The heat rate was 10°C min^{-1} before 400°C and then 2°C min^{-1} to 700°C.

2.2. Fabrication of $LiFePO_4$/Carbon Composite ($LiFePO_4$/C). All the experimental procedures did not change until the formation of a uniform sol. After forming the sol, 4.4 mL of aniline was added into the sol, followed by another stirring and reaction process for 3 hours. During this process, the redox reaction for coating polyaniline took place. The parameters of the solvent evaporation and heat treatment processes did not change either.

2.3. Characterizations. The phase structure of the products was determined by powder X-ray diffraction on a Bruker AXS D8-FOCUS diffractometer with Cu Kα radiation. The morphology and particle sizes were observed by field emission scanning electron microcopy (FDAC SU8010). Thermogravimetry/differential scanning calorimetry curves were obtained using STA 449F3 analyzer (NETZSCH) in the temperature range of 30~1000°C, using alumina crucible under nitrogen atmosphere and heating rate of 10°C min^{-1}.

2.4. Electrochemical Measurements. Test cells were fabricated utilizing active materials ($LiFePO_4$ and $LiFePO_4$/C) with acetylene black and polyvinylidene difluoride (PVDF) as the working electrode. Active material (85 wt.%), acetylene black (10 wt.%), and PVDF binder (5 wt.%) were dispersed in N-methyl-2-pyrrolidinone (NMP) solvent and ground thoroughly to form a slurry. Then the slurry was spread onto aluminum foil and maintained at 65°C in oven overnight. Metallic lithium plate was used as the counter electrode. The long-term galvanostatic charge/discharge was evaluated with an Arbin BT2000 multichannel galvanostat in the potential range of 2.5~4.2 V (versus Li/Li^+) at current densities of 34 mA g^{-1} and 850 mA g^{-1} (0.2 C and 5 C). CV and EIS were conducted on a Vmp3 (Biologic) electrochemical workstation. CV tests were done between 2.5 and 4.2 V (versus Li/Li^+) at the scan rate of 0.5 mV s^{-1}. EIS measurements were carried out over a frequency range of 10^5 ~10^{-2} Hz using a sine wave of 5 mV.

3. Results and Discussion

Figure 1(a) shows the 2nd cycle of galvanostatic charge/discharge curves of $LiFePO_4$ and $LiFePO_4$/C at 0.2 C. The $LiFePO_4$ delivered a capacity of 102.2 mAh g^{-1}, while the

$LiFePO_4$/C delivered a capacity as high as 117.1 mAh g^{-1} with a coulombic efficiency of 99.2%. The relative low specific capacity was calculated based on the composite of $LiFePO_4$ and carbon and could be explained by the high carbon content (~18.6%) of $LiFePO_4$/C obtained from the comparison of TG/DSC curves of $LiFePO_4$ and $LiFePO_4$/C shown in Figure 2 (the carbon content of our $LiFePO_4$/C was calculated from weight loss of the composite and this method was also reported by Lee et al. [17]). It is obviously showed that, comparing to $LiFePO_4$, the longer platforms of charge/discharge curves of $LiFePO_4$/C are almost parallel to each other from the beginning to the end, and the difference between the voltages of platforms is also much smaller, which represented better reversible performance, indicating decreased polarization. Electrochemical polarization was decreased because of fast electrons provided by carbon layers of high quality. Controlled particle size offered short diffusion distance for Li^+ in the solid state and large specific surface areas with abundant active sites for Li^+ to intercalate or deintercalate and concentration polarization was decreased in this way. With better reversible performance, the cycling performance of $LiFePO_4$/C is also notable even at high rate (5 C). As shown in Figure 1(b), with less than 9.5% discharge capacity loss over 2000 cycles, the coulombic efficiency maintained about 100%. The excellent cycling performance of our $LiFePO_4$/C is comparable with many other reports [15, 18, 19] and is closely associated with the structure produced by the carbon coating step involving redox reactions during the sol-gel process. The carbon coating process took place when the sol formed, as shown in Figure 3. After all the raw materials except aniline were mixed together and stirred for several hours, a uniform sol was formed. As there is O_2 in the air, amounts of ferrous ions were oxidized to ferric ions inevitably. The ferric ions were adsorbed to the surface of sol molecules due to the adsorption nature (the adsorption of charge particles) of sol. As a result of electrostatic interaction, all the ferric ions adsorbed distributed on the surface of the sol molecules uniformly and densely (state A). The polymerization of aniline is an oxidation process and ferric ions on the surface of sol molecules act as active sites for this oxidation reaction because the reduction process of ferric ions can coordinate with the oxidation process. That is to say the active sites for polymerization of aniline distributed on the surface of the sol molecules uniformly and densely. Aniline molecules have equal possibility to polymerize at anywhere on the surface of the sol molecules (state B). Thus, uniform, compact and intact polyaniline layers can be obtained by the cooperation between the polymerization of aniline (the oxidation process) and the reduction of ferric ions (state C). Finally, the same uniform, compact, and intact carbon layers coated on every single $LiFePO_4$ particle can be obtained after the calcining process (state D), instead of carbon layer with several agglomerated $LiFePO_4$ particles inside (state E) due to agglomeration caused by the high surface energy of the nanosized particles [13] or $LiFePO_4$ particles partially coated by carbon.

The FESEM picture shows irregular morphology of $LiFePO_4$ particles (Figure 4(a)). Although there are some

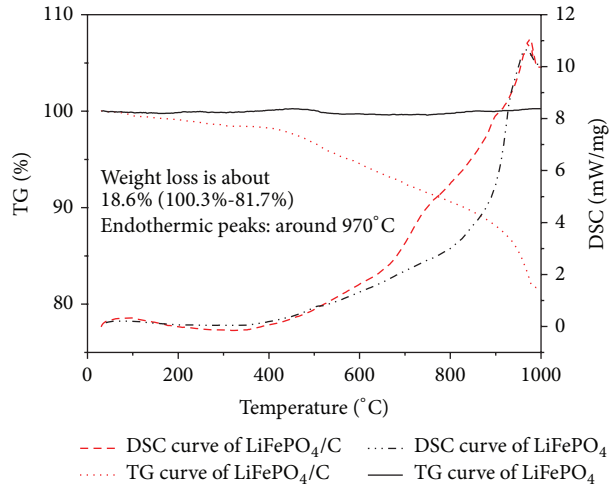

Figure 2: TG/DSC curves of $LiFePO_4$ and $LiFePO_4$/C.

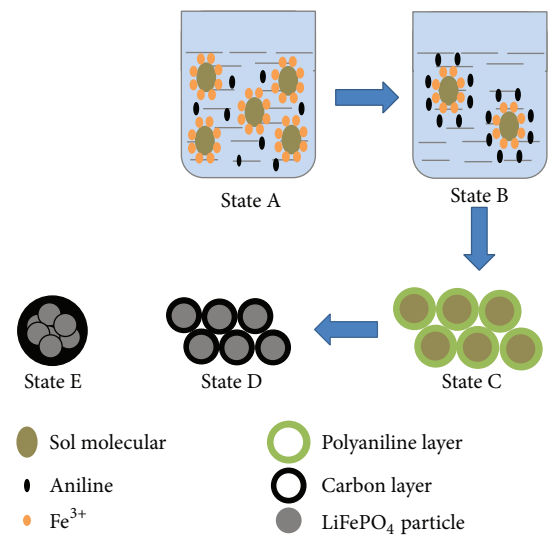

Figure 3: Scheme of formation process of interconnected $LiFePO_4$/C particles.

particles with the size of ~50 nm, these particles are not independent, but parts of much larger clusters and truly independent particles are not smaller than 500 nm. Comparing with $LiFePO_4$, the particles of $LiFePO_4$/C composite become much smaller and this huge change of morphology is mainly caused by the obtained carbon layers of high quality, which restrict the growth of $LiFePO_4$ and avoid the agglomeration of bare $LiFePO_4$ nanoparticles. As shown in Figure 4(b), with the size of ~50 nm, $LiFePO_4$/C nanoparticles interconnect with each other compactly, forming 3D continuous conductive structure. This is the very structure desired, which is shown as state D in Figure 3. In this optimized structure, electrons from multidimension can reach the $LiFePO_4$ particles immediately. The sluggish diffusion of Li^+ in the solid state accelerated as a result of the shortened diffusion distance in smaller particles.

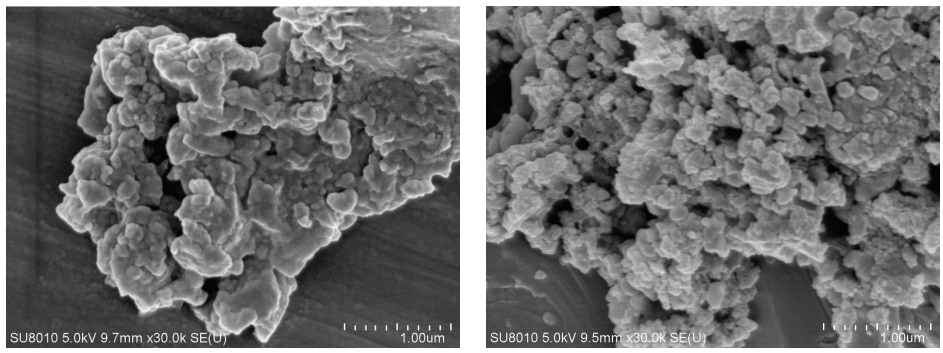

(a) (b)

Figure 4: FESEM micrographs of samples: (a) SEM micrographs of $LiFePO_4$ and (b) SEM micrographs of $LiFePO_4$/C.

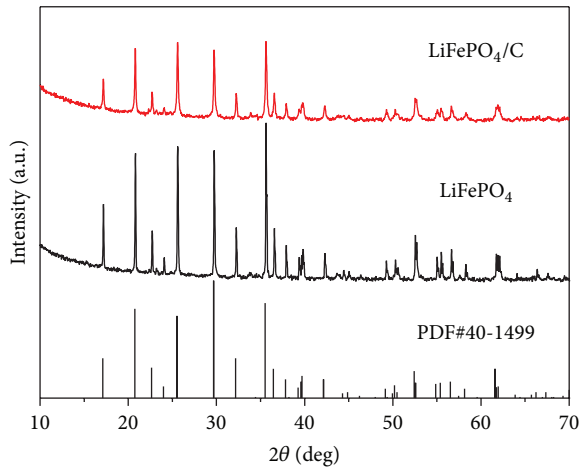

Figure 5: XRD patterns of $LiFePO_4$ and interconnected $LiFePO_4$/C particles.

The crystallographic structure determined by XRD further confirmed the smaller particle size after carbon coating. As shown in Figure 5, the widths of the major diffraction peaks turn to be bigger after carbon coating, indicating smaller particle size of $LiFePO_4$/C (according to Scherrer's formula). This phenomenon which is consistent with FESEM observations affirmed the main functions of the carbon layers, namely, the function of controlling particle size and avoiding agglomeration. From XRD patterns of the obtained $LiFePO_4$ and $LiFePO_4$/C, we can also see that all dominant diffraction peaks of $LiFePO_4$ and $LiFePO_4$/C samples can be indexed to orthorhombic $LiFePO_4$ (JCPDS card number 40-1499), indicating a perfect crystallinity of the as-synthesized samples. Besides, there is no evidence for the formation of amorphous carbons for the $LiFePO_4$/C.

As shown in Figure 6(a), a couple of redox peaks were observed for both $LiFePO_4$ and $LiFePO_4$/C in the CV curves obtained at a scan rate of 0.5 mV s^{-1}. Compared to $LiFePO_4$, the smaller peak potential difference of $LiFePO_4$/C indicates better reversibility, which is brought about by the decreased polarizations just mentioned (Figure 1(a)). Much higher peak currents are also shown, indicating faster reaction rate of $LiFePO_4$/C, and further confirmed the advantage of the interconnected structure, which provided electrode reactions of fast electrons and Li^+. Figure 6(b) presents the typical EIS responses of $LiFePO_4$ and $LiFePO_4$/C. Both of the Nyquist plots are composed of a depressed semicircle in the high-frequency region followed by a slanted line in the low-frequency region.

Referring to reported methods [20] and based on our EIS measurements, impedance parameters were calculated and listed in Table 1. The equivalent circuit diagram is shown in Figure 7.

The Warburg coefficient σ_ω can be obtained by

$$Z_{re} = R_e + R_{ct} + \sigma_\omega \omega^{-0.5}, \quad (1)$$

where R_e is the resistance of the electrolyte, R_{ct} is the charge transfer resistance, and ω is the angular frequency in the low-frequency region. Both R_e and R_{ct} are kinetic parameters independent of frequency. So σ_ω is the slope for the plot of Z_{re} versus the reciprocal root square of the lower angular frequencies ($\omega^{-0.5}$); as shown in Figure 8, the slope of the fitted line is the Warburg coefficient σ_ω.

The diffusion coefficient values of the lithium ions (D) can be obtained from

$$D = \frac{R^2T^2}{2A^2n^4F^4C^2\sigma^2}, \quad (2)$$

where R is the gas constant (8.314 J mol^{-1} K^{-1}), T is the temperature (298.5 K), A is the area of the electrode surface (2.0106 cm^2), F is Faraday's constant (96,500 C mol^{-1}), C is the molar concentration of Li^+ (1.09 mol L^{-1}), and n is the number of electrons transferred in the electrode reactions (for $LiFePO_4$, $n = 1$).

The conductivity values (σ) are calculated from

$$\sigma = \frac{1}{R_{ct}} \cdot \frac{t}{A}, \quad (3)$$

where t is the thickness of the cathode (250 μm).

The values of the exchange current density (i^0) are calculated from

$$i^0 = \frac{RT}{nFR_{ct}}. \quad (4)$$

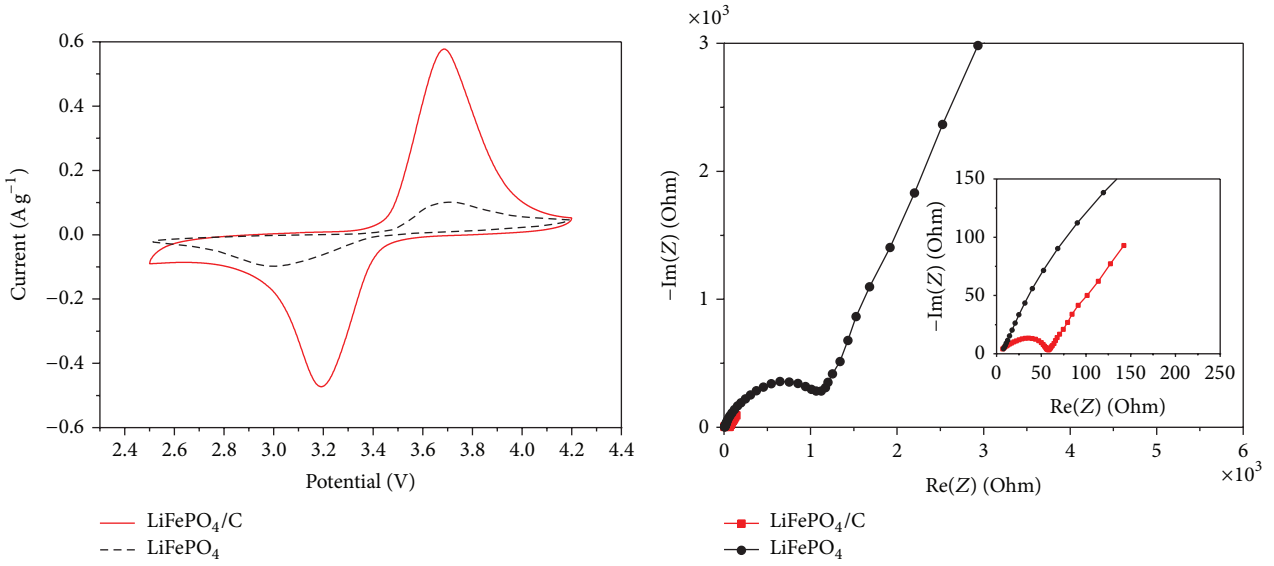

FIGURE 6: Electrochemical measurements of prepared samples: (a) CV curves of $LiFePO_4$ and the interconnected $LiFePO_4$/C nanoparticles in a voltage range of 2.5~4.2 V at a scanning rate of 0.5 mV s^{-1}. (b) Comparison of impedance spectra of $LiFePO_4$ and $LiFePO_4$/C.

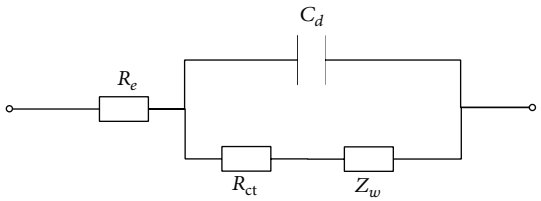

R_e: the resistance of the electrolyte
R_{ct}: charge transfer resistance
Z_w: Warburg resistance
C_d: double layer capacitance

FIGURE 7: Equivalent circuit diagram used in the calculation of impedance parameters.

The double layer capacitance C_d is determined by

$$C_d = \frac{1}{\omega R_{ct}}. \quad (5)$$

Comparing all the impedance parameters of $LiFePO_4$/C and $LiFePO_4$, we can see there is no big difference of R_e between the two samples, because the whole system and operation conditions were kept the same. While the values of R_{ct} and σ_ω changed dramatically, several orders of magnitude increases of D, σ, and i^0 were observed for $LiFePO_4$/C. All the changes reflected from the parameters listed in Table 1 can be explained from the aspect of structure. With uniform carbon layers on every single nanoparticle, all the nanoparticles interconnected with each other, forming 3D conductive network. The value of conductivity increases because electrons can diffuse from all directions. Diffusion of Li^+ in the solid state becomes much faster in nanoparticles with controlled size, leading to the increase of the diffusion coefficient

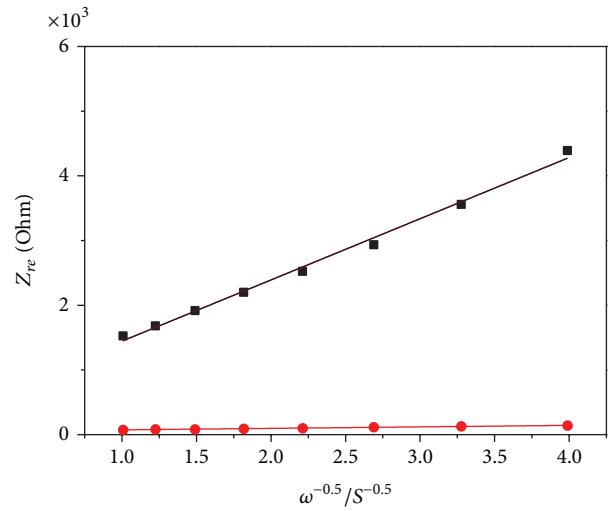

$LiFePO_4$	Intercept	498.65849
	Slope	946.20855
$LiFePO_4$/C	Intercept	50.56364
	Slope	23.15497

FIGURE 8: The relationship between Z_{re} and $\omega^{-0.5}$ at low frequencies for $LiFePO_4$ and $LiFePO_4$/C samples.

value of Li^+ and reduction of Warburg impedance. Both electrons and Li^+ can respond to the electrode reactions immediately, minimizing the electrochemical polarization and concentration polarization. What is more, according to some research, polyaniline contains element N, which can also

Table 1: Impedance parameters of the samples.

Samples	R_e/Ω	R_{ct}/Ω	C_d/F	$\sigma_\omega/\Omega\,\mathrm{cm}^2\,\mathrm{s}^{-0.5}$	$D/\mathrm{cm}^2\,\mathrm{s}^{-1}$	$\sigma/\mathrm{S\,cm}^{-1}$	$i^0/\mathrm{mA\,cm}^{-2}$
$LiFePO_4/C$	9.3	41.3	2.2×10^{-4}	23.2	1.4×10^{-11}	3.0×10^{-4}	6.2×10^{-4}
$LiFePO_4$	10.5	488.2	3.7×10^{-7}	946.2	8.3×10^{-15}	2.5×10^{-5}	5.3×10^{-5}

affect the electrochemical performance [21]. That is why the values of exchange current density increased and the charge transfer resistance decreased and our $LiFePO_4/C$ sample exhibited notable cycling performance even at high rate.

Analysis based on all the parameters confirmed the results of CV and galvanostatic charge/discharge tests, which suggests that our carbon coating method is ingenious, efficient, and preferred and can result in ideal structure with carbon layers of high quality.

In addition to shortening the diffusion distance of Li^+, the controlled particle size can also improve the utilization of active materials. In the lattice of $LiFePO_4$, Li^+ migrates through one-dimensional channels [5, 22–24]. Cross-channel diffusion of Li-ion happens with the help of antisite defects [25, 26], but, with several immobile point defects (such as $Fe^{\bullet}_{Li}$, a kind of defects: one ferrous ion occupies the lattice position of lithium ion) in a single channel, Li^+ sites situated between immobile point defects cannot be reached, which causes "blocked" capacity. In very large particles most sites will be blocked by defects in this way, while the total channel length between surfaces in nanoparticles is small, resulting in channels containing very few or even zero defects. For instance, for particles smaller than 60 nm, 1% $Fe^{\bullet}_{Li}$ population leads to on average fewer than two defects residing in each channel and therefore no "blocked" Li^+ sites [26]. For our interconnected $LiFePO_4/C$ nanoparticles with an average diameter around 50 nm, there are less immobile point defects, which minimized the "blocked" capacity and improved the utilization of active materials.

Our carbon coating process is based on a couple of redox reactions following the formation of $LiFePO_4$ sol. Owing to the redox reactions, the position of carbon layer was fixed, the thickness of the carbon layer was limited, and the uniformity of the carbon layer was guaranteed. Finally, the target structure formed. With high quality carbon layers and controlled particle size, the electronic conductivity (σ), the diffusion coefficient of Li^+ (D), and the exchange current density (i^0) all increased. Obviously, for the same purpose of ensuring the homogeneous distribution of carbon, our method turns to be more convenient, more efficient, and more ingenious. Because no surfactant is used, no complex experiments operations are needed and high cycling performance mentioned above is presented.

4. Conclusions

In conclusion, interconnected $LiFePO_4$/carbon nanoparticles were synthesized successfully in our work. By an ingenious, efficient, and convenient method involving a couple of redox reactions, the structure of uniform, compact, and intact carbon layer on every single $LiFePO_4$ nanoparticle was obtained. The high quality carbon layers coated on every $LiFePO_4$ particle not only acted as protection layers but also provided fast electrons for electrode reactions by forming 3D conductive network. The proper particle size controlled offered Li^+ shorter diffusion distance, accelerating the diffusion of Li^+ in the solid state. And the large specific surface area ensured the sufficient contact between the electrode material and electrolyte. Considering the existence of immobile point defects, the utilization of active materials was also improved. The synergistic effect of high quality carbon layers and controlled particle size decreased the electrochemical polarization and concentration polarization, making the reaction rate fast enough to exhibit dramatically improved electrochemical performance including remarkable cycling performance at high rate.

Conflict of Interests

The authors declare that there is no conflict of interests regarding the publication of this paper.

Acknowledgments

This work was supported by the National Natural Science Foundation of China (21173198) and the Science and Technology Support Program of Hubei Province, China (2013BHE014).

References

[1] A. K. Padhi, K. S. Nanjundaswamy, and J. B. Goodenough, "Phospho-olivines as positive-electrode materials for rechargeable lithium batteries," *Journal of the Electrochemical Society*, vol. 144, no. 4, pp. 1188–1194, 1997.

[2] A. Padhi, K. Nanjundaswamy, C. Masquelier, S. Okada, and J. B. Goodenough, "Effect of structure on the Fe^{3+}/Fe^{2+} redox couple in iron phosphates," *Journal of the Electrochemical Society*, vol. 144, no. 5, pp. 1609–1613, 1997.

[3] F. Yu, S. Ge, B. Li, G. Sun, R. Mei, and L. Zheng, "Three-dimensional porous $LiFePO_4$: design, architectures and high performance for lithium-ion batteries," *Current Inorganic Chemistry*, vol. 2, no. 2, pp. 194–212, 2012.

[4] M. Wagemaker, B. L. Ellis, D. Lützenkirchen-Hecht, F. M. Mulder, and L. F. Nazar, "Proof of supervalent doping in olivine $LiFePO_4$," *Chemistry of Materials*, vol. 20, no. 20, pp. 6313–6315, 2008.

[5] C. A. Fisher, V. M. Prieto, and M. S. Islam, "Lithium battery materials $LiMPO_4$ (M = Mn, Fe, Co, and Ni): insights into defect association, transport mechanisms, and doping behavior," *Chemistry of Materials*, vol. 20, no. 18, pp. 5907–5915, 2008.

[6] X.-L. Wu, Y.-G. Guo, J. Su, J.-W. Xiong, Y.-L. Zhang, and L.-J. Wan, "Carbon-nanotube-decorated nano-$LiFePO_4$@C cathode

material with superior high-rate and low-temperature performances for lithium-ion batteries," *Advanced Energy Materials*, vol. 3, no. 9, pp. 1155–1160, 2013.

[7] J. Yang, J. Wang, Y. Tang et al., "In situ self-catalyzed formation of core-shell $LiFePO_4$@CNTs nanowires for high rate performance lithium-ion batteries," *Journal of Materials Chemistry A*, vol. 1, no. 25, pp. 7306–7311, 2013.

[8] L. Fei, Y. Xu, X. Wu et al., "Instant gelation synthesis of 3D porous MoS_2@C nanocomposites for lithium ion batteries," *Nanoscale*, vol. 6, pp. 3664–3669, 2014.

[9] L. Fei, Q. Lin, B. Yuan et al., "Reduced graphene oxide wrapped fes nanocomposite for lithium-ion battery anode with improved performance," *ACS Applied Materials and Interfaces*, vol. 5, no. 11, pp. 5330–5335, 2013.

[10] R. Dominko, M. Bele, M. Gaberscek et al., "Porous olivine composites synthesized by sol-gel technique," *Journal of Power Sources*, vol. 153, no. 2, pp. 274–280, 2006.

[11] S. Wang, H. Yang, L. Feng et al., "A simple and inexpensive synthesis route for $LiFePO_4$/C nanoparticles by co-precipitation," *Journal of Power Sources*, vol. 233, pp. 43–46, 2013.

[12] R. Yi, F. Dai, M. L. Gordin, S. Chen, and D. Wang, "Micro-sized si-c composite with interconnected nanoscale building blocks as high-performance anodes for practical application in lithium-ion batteries," *Advanced Energy Materials*, vol. 3, no. 3, pp. 295–300, 2013.

[13] H. Li and H. Zhou, "Enhancing the performances of li-ion batteries by carbon-coating: present and future," *Chemical Communications*, vol. 48, no. 9, pp. 1201–1217, 2012.

[14] J. Yang, J. Wang, Y. Tang et al., "$LiFePO_4$–graphene as a superior cathode material for rechargeable lithium batteries: impact of stacked graphene and unfolded graphene," *Energy and Environmental Science*, vol. 6, no. 5, pp. 1521–1528, 2013.

[15] Y. Wang, Y. Wang, E. Hosono, K. Wang, and H. Zhou, "The design of a $LiFePO_4$/carbon nanocomposite with a core-shell structure and its synthesis by an in situ polymerization restriction method," *Angewandte Chemie*, vol. 47, no. 39, pp. 7461–7465, 2008.

[16] J. Wang and X. Sun, "Understanding and recent development of carbon coating on $LiFePO_4$ cathode materials for lithium-ion batteries," *Energy and Environmental Science*, vol. 5, no. 1, pp. 5163–5185, 2012.

[17] S.-H. Lee, M.-J. Jung, J.-S. Im, K.-Y. Sheem, and Y.-S. Lee, "Preparation and characterization of electrospun $LiFePO_4$/carbon complex improving rate performance at high C-rate," *Research on Chemical Intermediates*, vol. 36, no. 6-7, pp. 591–602, 2010.

[18] X. Yan, G. Yang, J. Liu et al., "An effective and simple way to synthesize $LiFePO_4$/C composite," *Electrochimica Acta*, vol. 54, no. 24, pp. 5770–5774, 2009.

[19] J. Liu, J. Wang, X. Yan et al., "Long-term cyclability of $LiFePO_4$/carbon composite cathode material for lithium-ion battery applications," *Electrochimica Acta*, vol. 54, no. 24, pp. 5656–5659, 2009.

[20] Y. Cui, X. Zhao, and R. Guo, "Improved electrochemical performance of $La_{0.7}Sr_{0.3}MnO_3$ and carbon co-coated $LiFePO_4$ synthesized by freeze-drying process," *Electrochimica Acta*, vol. 55, no. 3, pp. 922–926, 2010.

[21] G. Ćirić-Marjanovic, I. Pašti, N. Gavrilov, A. Janošević, and S. Mentus, "Carbonised polyaniline and polypyrrole: towards advanced nitrogen-containing carbon materials," *Chemical Papers*, vol. 67, no. 8, pp. 781–813, 2013.

[22] J. Yang and J. S. Tse, "Li ion diffusion mechanisms in $LiFePO_4$: an ab initio molecular dynamics study," *Journal of Physical Chemistry A*, vol. 115, no. 45, pp. 13045–13049, 2011.

[23] P. Zhang, Y. Wu, D. Zhang et al., "Molecular dynamics study on ion diffusion in $LiFePO_4$ olivine materials," *Journal of Physical Chemistry A*, vol. 112, no. 24, pp. 5406–5410, 2008.

[24] J. Hong, X. Wang, Q. Wang et al., "Structure and electrochemistry of vanadium-modified $LiFePO_4$," *Journal of Physical Chemistry C*, vol. 116, no. 39, pp. 20787–20793, 2012.

[25] G. K. P. Dathar, D. Sheppard, K. J. Stevenson, and G. Henkelman, "Calculations of Li-ion diffusion in olivine phosphates," *Chemistry of Materials*, vol. 23, no. 17, pp. 4032–4037, 2011.

[26] R. Malik, D. Burch, M. Bazant, and G. Ceder, "Particle size dependence of the ionic diffusivity," *Nano Letters*, vol. 10, no. 10, pp. 4123–4127, 2010.